

Comparative study of optical sources in the near infrared for optical coherence tomography applications

Lionel Carrion
Michel Lestrade
Zhiqiang Xu
Gaby Touma
Romain Maciejko

École Polytechnique de Montréal
Department of Engineering Physics
Optoelectronics Laboratory
P.O. Box 6079, Station "Centre-ville"
Montréal, Québec H3C 3A7 Canada
E-mail: lionel.carrion@polymtl.ca

Michel Bertrand

École Polytechnique de Montréal
Institute of Biomedical Engineering
P.O. Box 6079, Station "Centre-ville"
Montréal, Québec H3C 3A7 Canada

Abstract. Optical coherence tomography (OCT) is a powerful, non-invasive biomedical technique that uses low-coherence light sources to obtain in-depth scans of biological tissues. We report results obtained with three different sources emitting at 1570, 1330, and 810 nm, respectively. Attenuation and backscattering measurements are obtained with these sources for several *in vitro* biological tissues. From these measurements, we use a graphical method to make comparisons of the penetration depth and backscattering intensity of each wavelength for the studied samples. The influence of the coherence length of each source is also taken into account in order to make a more relevant comparison. © 2007 Society of Photo-Optical Instrumentation Engineers. [DOI: 10.1117/1.2710242]

Keywords: coherent optical systems; medical imaging; optical properties; attenuation; absorption.

Paper 06051R received Mar. 7, 2006; revised manuscript received Jul. 27, 2006; accepted for publication Oct. 1, 2006; published online Feb. 23, 2007. This paper is a revision of a paper presented at the SPIE conference on Photonic Applications in Biosensing and Imaging, Sep. 2005, Toronto, Canada. The paper presented these appears (unrefereed) in SPIE proceedings Vol. 5969.

1 Introduction

Optical coherence tomography (OCT) is an imaging technique that appeared about 15 years ago.¹ It is based on the interferometric analysis of low-coherence light backscattered from inhomogeneities inside a tissue. It can provide in-depth profiles of tissues with a resolution of the order² of 1 μm . Since it offers a noninvasive and noncontact approach, OCT is gaining acceptance as a prominent medical imaging technique especially for ophthalmic applications. Recent developments in the OCT domain aimed at improving several characteristics such as resolution, signal-to-noise ratio (SNR), or penetration depth. These are key parameters for improving OCT efficiency in the detection of pathologies such as tumors inside highly scattering organs and tissues (e.g., skin, heart, or liver). These parameters are strongly related to the light source characteristics, especially to its emission wavelength λ_c and bandwidth $\Delta\lambda$. As shown by the equation $\Delta z = [2 \ln(2)\lambda_c^2]/(\pi\Delta\lambda)$, a light source with a broader bandwidth results in an improvement of the OCT axial resolution Δz (also called the coherence length of the light source). As there is a strong spectral dependency of tissue optical properties such as absorption and scattering coefficients, OCT penetration depth and contrast are mainly related to the emission wavelength of the source. Previous studies were based on the comparison of images obtained with two different wavelengths, mostly at both 800 and 1300 nm, showing^{3,4} a better penetration depth at 1300 nm. Several authors predicted

penetration depths in several tissues for various optical sources, but these results were not confirmed experimentally.⁵

In this paper, we propose a more complete investigation with comparison of images obtained with three different optical sources at 810-, 1330-, and 1570-nm emission wavelengths with a better coverage of the near-IR band. Along with a qualitative comparison of images, we used a graphical method⁶ to measure attenuation and backscattering coefficients from OCT in-depth profiles of miscellaneous *in vitro* biological samples. From these measurements, we deduced comparisons of the performance of each emission wavelength, especially on the penetration depth and backscattering intensity for the studied samples. The influence of coherence length is then taken into account to make a more detailed comparison of the sources used in this experiment.

2 Experimental Setup

Our OCT setup is based on three different sources used with different Michelson interferometers. The first source is a Kerr-lens mode-locking, ultrashort pulsed Ti:sapphire laser that gives a maximum bandwidth of 100 nm at an about 810-nm central wavelength. In this configuration, we measure a coherence length of 3.5 μm . The second one uses nonlinearly transformed light from a high-power laser to produce broadband, high-power continuous light in the near-IR region (BBS series from MPB Communications, Inc.). Its emission spectrum is centered near 1330 nm with a 100-nm bandwidth, leading to a coherence length of 8 μm . The third source is a superluminescent diode (SLD) from JDS Uniphase, Inc. that emits a 60-nm bandwidth spectrum at a 1570-nm central wavelength. Its coherence length is equal to 22 μm . Spectra

Address all correspondence to Lionel Carrion, Engineering Physics, Ecole Polytechnique de Montreal, P.O. Box 6079, Station Centre Ville Montreal, QUEBEC H3C3A7 Canada; Tel: 514 340 4711 (#4489); Fax: 514 340 3218; E-mail: lionel.carrion@polymtl.ca.

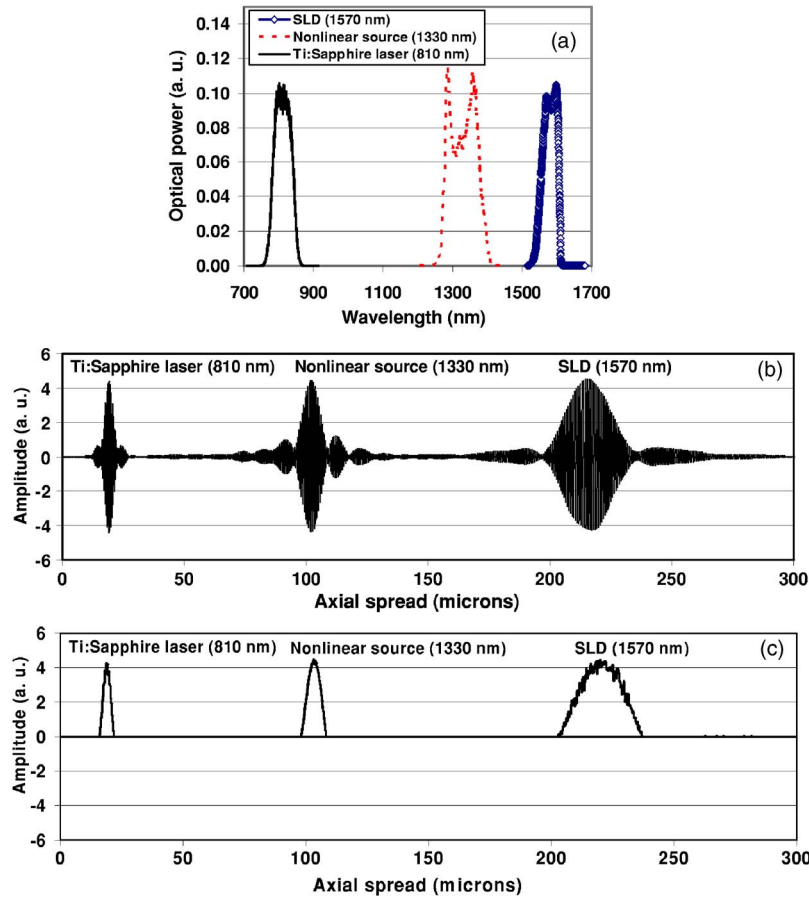


Fig. 1 (a) Spectra of the sources used for experiments, (b) OCT response obtained with each source and setup, and (c) OCT response of each setup treated with the deconvolution method presented in Sec. 3.

of the sources are shown in Fig. 1, along with the OCT response of each system measured with a mirror surface used as a sample inside the interferometers. Note here that although the coherence lengths of each source were measured from the FWHM of the OCT traces, the presence of sidelobes on each side may deteriorate the tissue profile quality. These sidelobes are related to the deviation of the source spectrum from a perfect Gaussian shape. We can see from Fig. 1(b) that sidelobes are large for the 1330-nm source (where the sidelobe amplitude is almost 30% of the total OCT amplitude) and for the 1570-nm SLD (where the width of each sidelobe is about $30 \mu\text{m}$). For the Ti:sapphire laser, the spectrum is close to a Gaussian such that the sidelobes are narrower than for the other sources.

The layout of the setup is depicted in Fig. 2. A free-space interferometer is used with the Ti:sapphire laser. For the 1330- and 1570-nm sources, we use customized fiber interferometer modules (1330-OCTM and 1570-OCTM). SMF-28 fibers with polarization controllers were used. Each of these modules is optimized to fit the spectral domain of each source. For each source light is focused onto the samples with near-IR, achromatic low-numerical aperture (NA, 0.25 NA, $10\times$ magnification) microscope objectives in order to get a wide depth of field. Data acquisition consists of balanced detection, analog envelope detection and analog-to-digital (A/D) conversion with a digital multimeter. For efficient balanced detection, the

two incoming waves on the detector must be in phase quadrature. This condition is achieved with a polarizing cube coupled with a HWP and a QWP in the free-space interferometer, and with a broadband fiber circulator in the fiber interferometer. The sample under test is covered with a thin glass coverslip. It is then placed inside a chamber filled with saline solution for better preservation. To match the SNRs of each source as closely as possible, the following procedure was implemented before the experiments. First, we inserted a biological tissue in the sample arm of the interferometer. The reflected power from the reference and the sample arm were then approximately equalized by inserting neutral density filters in both arms. Care was taken that the thickness of density filters was the same in both arms in order to limit the dispersion mismatch. We checked that this ratio was roughly the same for each source. Then, the OCT response of each system was measured by placing in the sample arm a totally reflective gold mirror whose reflectivity was assumed to be the same for each wavelength used throughout. The input power of each source was independently modified with neutral density filters to achieve the same OCT response amplitude for each system, thus removing the wavelength dependence of the detector quantum efficiency. Hence, under the shot-noise limit induced by balanced detection, the SNR difference between the three systems is minimized.

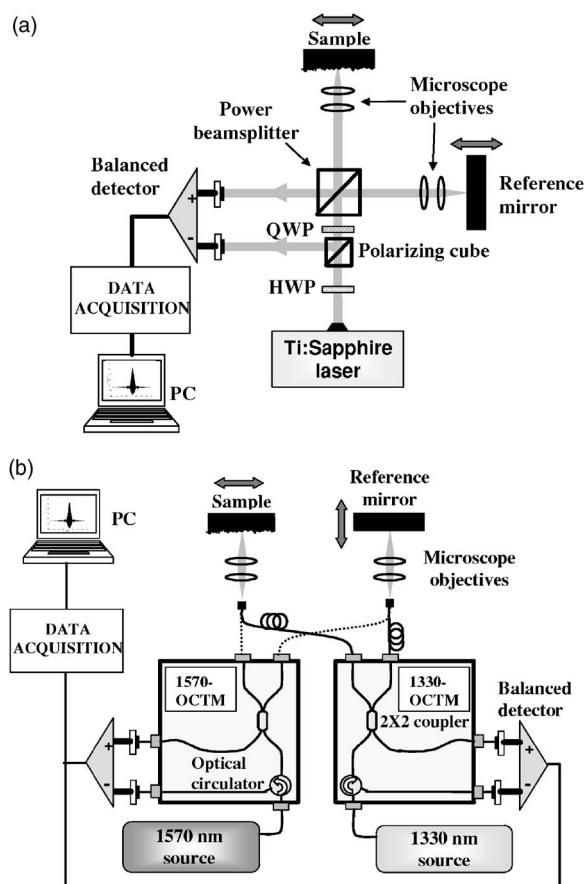


Fig. 2 OCT setup: (a) free-space interferometer used with Ti:sapphire laser (HWP, half-wave plate; QWP, quarter-wave plate) and (b) fiber interferometers used with 1330- and 1570-nm sources.

3 Results and Discussion

Light propagation inside the sample is assumed to be described by the Beer-Lambert law:

$$P_T(z) = P_0 \exp(-\alpha_T z), \quad (1)$$

where P_0 and $P_T(z)$ are the incident optical power and the transmitted power after propagating through a medium thickness of z , respectively. The coefficient α_T represents the whole attenuation of the medium. For shallow depths in turbid tissue, the approximation can be made that the absorption and scattering coefficients α_a and α_s are the main contributions to attenuation:⁶

$$\alpha_T = \alpha_a + \alpha_s. \quad (2)$$

Obviously, the penetration depth is defined as the reciprocal of the attenuation coefficient.

For a qualitative comparison of penetration depth and contrast, images of *in vitro* samples were made with these three different sources. The samples were placed in such a way that the focus is located in the middle of the scan. For better visibility we chose inhomogeneous tissue. On the top row of Fig. 3 we show images from a fresh chicken heart ventricle wall. The bottom row shows a profile from a mouse earlobe that was fixed in formalin just after sacrifice. Because of the nu-

merous discontinuities generated by cartilage layers inside this sample, the “ringing” effect induced by important sidelobes for 1330- and 1570-nm sources can mask a lot of details. As a matter of fact, sidelobes can be a significant issue especially in the case of inhomogeneous tissues where discontinuities with various reflection coefficients are located very close to each other: sidelobes from strongly reflected signals can mask weakly reflected signals. Thus, we treated the mouse ear images obtained at 1330 and 1570 nm with a deconvolution method to remove the sidelobes from the OCT signal and thus improve image sharpness.⁷ While this method serves the same purpose as spectral shaping methods,⁸ it is based on an iterative deconvolution of the raw profile with the system OCT responses that are shown in Fig. 1(b). As shown in Fig. 1(c), where the deconvolution method was applied to the OCT traces of each source and system, it can bring an efficient sidelobe extinction of at least 20 dB, while the main OCT signal amplitude remains unchanged. The chicken heart sample is more homogeneous: within the sample, the masking effect induced by the sidelobes is weak and needs no special treatment. On the left, the images obtained with the Ti:sapphire laser show accurate details at shallow depths not only because the depth resolution is higher than with the other sources, but also because the backscattering seems to be higher. As these tissue are inhomogeneous, the nature of the backscattered power cannot be clearly defined: it mainly comes on the one hand from diffuse reflection generated by a large-scale index mismatch at inhomogeneities,⁹ and on the other hand from the statistical process of light scattering by an homogeneous ensemble of particles. Nevertheless we can notice that the 1330- and 1570-nm wavelengths still benefit from higher penetration depths (i.e., lower attenuations) despite the fact that absorption is assumed to be higher for these wavelengths: as can be seen in the images, the second layer of the ventricle wall is more visible at 1330 and 1570 nm, and the backscattered intensity is quite homogeneous over the whole mouse ear thickness at 1330 and 1570 nm, while it slightly decreases^{5,10} with depth at 810 nm. This statement implies via Eq. (2) that the sum of statistical and diffuse scattering decreases as wavelength increases and that its contribution to α_T may be more important than absorption. The semi-empirical law stating that statistical scattering behaves as an inverse power of the wavelength may be partly responsible for this.^{4,11} Nevertheless, there is also a strong contribution from diffuse reflections, so that we cannot draw an unambiguous conclusion about the backscattered light behavior as a function of wavelength.

In fact, a qualitative comparison is obviously limited by numerous factors. From these images, it is very difficult to compare the penetration depths for 1330- and 1570-nm sources and to define which one is the lowest. Furthermore, the aperture function of the microscope objectives is not taken into account. In other words, because the beam is focused inside the sample, the mixing of the probe and the reference beams in the interferometer is less efficient for in-depth cells that are far from focus, giving rise to a reduced OCT signal. The Rayleigh range is especially important for comparisons in Fig. 3, since it gives the distance from the focused beam waist for which the OCT amplitude decreases by a $2^{1/2}$ factor. Since the same microscope objectives were used for the three

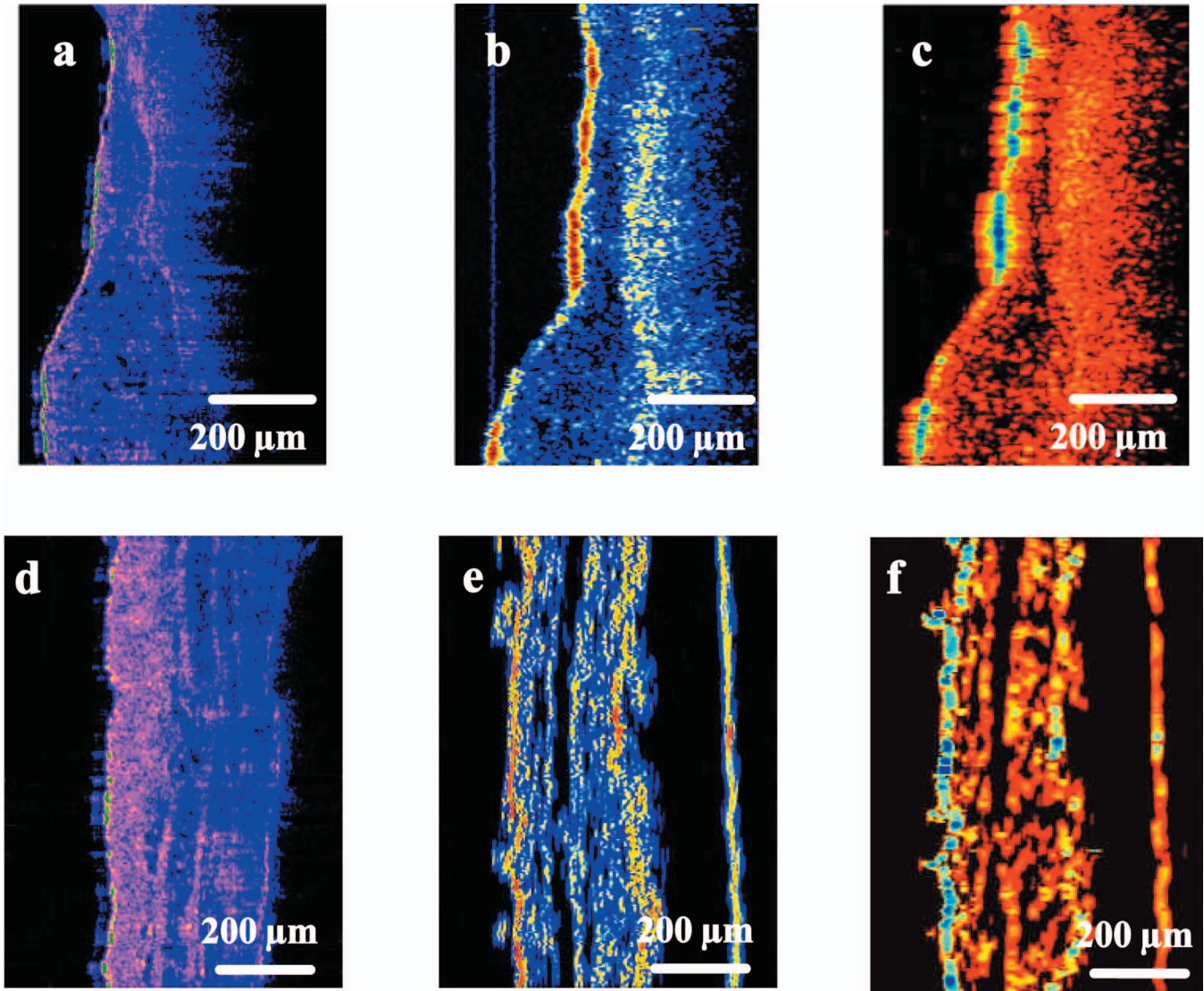


Fig. 3 OCT profiles of (a), (b), and (c) a chicken heart ventricle wall and (d), (e), and (f) mouse earlobe. From left to right, 810-nm Ti:sapphire laser, 1330-nm broadband source, and 1570-nm SLD. Each source was assigned a different color map that refers to its emission wavelength. Light is incident from the left.

sources, one might expect a lower Rayleigh range for 810 nm. As a consequence, it may be partly responsible for lower penetration depths observed on the images made with Ti:sapphire laser. Speckle noise is also a limiting factor since it introduces a granular image aspect that depends on the source coherence length. It is thus very difficult to make clear and definitive conclusions, and some precise measurements of attenuation and backscattering are necessary for more accurate comparisons. For this, we apply Eq. (1) to the reference OCT power P_{in}^{meas} measured from the glass-sample interface and the OCT power $P_{out}^{meas}(z')$ measured from an optical depth z' inside the sample. We obtain the following formula:³

$$\frac{P_{out}^{meas}(z')}{A(z')} = \frac{P_{in}^{meas}}{A_{in}} \frac{l_c}{2} \alpha_b \exp(-2\alpha_r z') \frac{T_{GS}^2}{R_{GS}}, \quad (3)$$

where α_b is the backscattering coefficient, and R_{GS} and T_{GS} are the reflection and transmission coefficients of the glass-sample interface and are given by

$$R_{GS} = \left(\frac{n_G - n_S}{n_G + n_S} \right)^2, \quad T_{GS} = \frac{4n_G n_S}{(n_G + n_S)^2}. \quad (4)$$

The refractive index of glass n_G is assumed to be equal to 1.51 for 810 nm and 1.50 for 1330 and 1570 nm. The refractive index of the sample n_S is measured for each source by placing the tissue that was previously soaked in a saline solution inside a cell made of a front glass coverslip and an end mirror. We then compared the OCT-measured optical thicknesses of the same cell with and without the tissue.¹² The refractive indices of the tissues were obtained by averaging the thickness ratio over the whole cell. For tissues studied in this paper, typical values between 1.39 and 1.42 were obtained with a typical error of 1%. An important point in Eq. (4) is that $P_{out}^{meas}(z')$ depends on the coherence length l_c . In a turbid media, adjacent scattering centers are separated by distances much shorter than the coherence length. Because of the width l_c of the OCT trace assigned to the reflection of each

Table 1 Rayleigh range in free space and focused beam diameter of the sources used in the experiments.

Source (nm)	Rayleigh Range (μm)	Focused Beam Diameter (μm)
810	77	9
1330	129	14.7
1570	147	17.1

scattering center the total OCT signal amplitude measured at one point of the depth scan arises not only from the scattering center at this point, but also from contributions of all the scattering centers that are located at distances less than l_c from this point.⁶ When the coherence length is much less than the photon mean free path in the tissue, and under the approximation of the Gaussian shape of the OCT function by a rectangular function of width l_c , this assertion is expressed through the factor $l_c/2$ in Eq. (3). Consequently, the measured backscattered intensity from one point inside the tissue depends on the coherence length. Note that $A(z')$ and A_{in} are corrective factors that represent the aperture function of the interferometer at z' and at the glass-sample interface, respectively. Hence, $A(z')$ is the ratio of the reduced OCT amplitude measured at z' and the maximum OCT amplitude measured at the focus point. This was estimated in free space by measuring OCT traces from a hard reflection off a totally reflective mirror that was inserted in the sample arm. First, we measure the amplitude of the OCT signal that is obtained when the mirror is placed at the focus of the objective. The OCT amplitude is then measured for different positions of this mirror from the beam focus. Measurements were made for each source. In the Gaussian beam approximation, the measured data points can be approximated by the following formula:

$$A(z) = 1/[1 + (z/w_R)^2]^{1/2}, \quad (5)$$

where $w_R = \pi w_{\text{min}}^2 / 4\lambda_c$ is the Rayleigh range, and w_{min} is the waist of the focused beam. These parameters are then deduced from data extrapolation with the form in Eq. (5) and are reported in Table 1. An aperture correction function in the sample is obtained straightforwardly by replacing z by $z' = n_S(z)$, or by noting that the equivalent Rayleigh range in the tissue is w_R/n_S . Typical errors in the aperture correction arise

from the standard deviations of the fit and from errors on refractive index measurements. They are found to be less than 5%. If we add the measurement errors that arise from R_{GS} and T_{GS} , typical errors in α_t and α_b run between 10 and 15%.

We can then rewrite Eq. (3) in the form

$$B(z') = \ln(\alpha_b) - 2\alpha_t z', \quad (6)$$

where

$$B(z') = \ln \left[\frac{P_{\text{out}}^{\text{meas}}(z') R_{\text{GS}} A_{\text{in}} \frac{2}{l_c}}{P_{\text{in}}^{\text{meas}} T_{\text{GS}}^2 A(z') l_c} \right]. \quad (7)$$

Attenuation and backscattering measurements come straightforwardly by plotting $B(z')$ as a function of optical depth z' for each OCT in-depth scan. For relatively shallow depths in the sample, the obtained curve is easily fitted by a straight line whose slope and offset give α_t and α_b , respectively. Figure 4(a) shows a typical $B(z')$ curve calculated from a single in-depth scan. As we go deeper into the sample, the curve slope tends to level off until $B(z')$ becomes a constant. We believe that this may be explained by the fact that the single-scattering assumption is no longer valid: due to multiple scattering effects the beam loses its spatial coherence and the aperture function is modified from its ideal Gaussian shape measured in free space.¹³ More precisely, the probability for a photon scattered once to be backscattered toward the detector can no longer be neglected. This is why the single-scattering model of Eq. (6) underestimates the backreflected power from deep centers. Nevertheless, the photon mean-free path exceeds several hundreds of micrometer in most biological tissues: even for highly scattering tissues such as skin, this degradation seldom occurs³ for depths less than 200 μm . Care was taken to check that the straightline fitting procedure was done over a region where the $B(z')$ curve has a roughly constant slope. Another cause of the OCT signal degradation may be the dispersion induced by the sample. As an approximation to biological samples, the effect of water-induced dispersion on OCT traces broadening has been investigated with various optical sources in a recent work.¹⁴ From this work, for thicknesses under 500 μm , we can predict for our sources characteristics a very weak broadening of the OCT trace. Dispersion effect is therefore neglected in our calculations.

Measurements of attenuation and backscattering coefficients were carried out on several *in vitro* tissue samples: chicken aorta intimal surface, chicken myocardium outer sur-

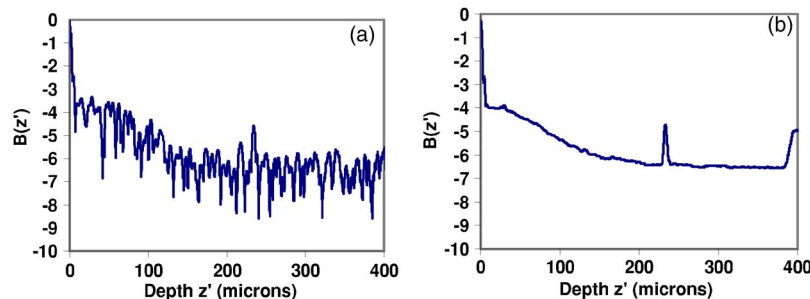


Fig. 4 Comparison of OCT profiles for (a) a single in-depth scan and (b) a spatially and temporally averaged in-depth scan. The pronounced peaks in the constant signal region are artifacts.

Table 2 Optical coefficients of several samples measured by OCT with 810=, 1330=, and 1570=nm sources.

Sample	Source (nm)	α_b (mm ⁻¹)	Standard Deviation (mm ⁻¹)	α_t (mm ⁻¹)	Standard Deviation (mm ⁻¹)
Chicken aorta	810	0.033	0.0073	9.13	0.99
	1330	0.0061	0.0021	6.13	1.59
	1570	0.0063	0.0033	6	2.23
Chicken myocardium	810	0.0039	0.0019	4.16	2.43
	1330	0.0012	0.00074	2.10	2.09
	1570	0.00097	0.00067	1.39	0.56
Chicken liver	810	0.0135	0.0052	11.17	2.27
	1330	0.0071	0.0037	2.1	0.13
	1570	0.0015	0.00023	2.07	0.32
Human skin	810	0.008	0.0036	8.12	2.27
	1330	0.0025	0.0014	6.2	1.96
	1570	0.0011	0.00071	3.9	2.68

face, chicken liver, and human epidermis in the finger tip region. These samples were more homogeneous than those chosen in Fig. 3. Aorta, myocardium, and liver were placed after sacrifice inside a refrigerator for several hours before experimental study. Skin was taken from an *in vivo* human finger tip and was studied immediately after excision. In-depth scans were performed on 150 equidistant transverse sites over a transverse range of 750 μm . This means that two adjacent measured sites are separated by a distance of 5 μm . Although this distance is lower than the focused beam diameter, the overlap between two adjacent probed volumes is limited, and each transverse scan is considered to be independent from each other. Spatial averaging over the whole transverse range is thus possible for speckle noise reduction.^{15,16} Moreover, this procedure further reduces the local irregularities induced by inhomogeneities. Each in-depth scan was also repeated five times and then temporally averaged for electronic noise reduction.¹⁶ This resulted in an efficient noise reduction of roughly 30 dB, as shown in Fig. 4.

Attenuation and backscattering coefficients were obtained from Eqs. (6) and (7) and are given in Table 2. Mean values are obtained from fitting the spatially and temporally averaged in-depth scan for each sample. Standard deviations are calculated from statistics of the coefficients measured at each transverse point. Hence, they provide useful information concerning tissue structure and homogeneity. Liver tissue is the most homogeneous of the four samples studied in this paper. This is confirmed by the weak standard deviations measured for this sample. Skin tissue has a more stratified nature, while myocardium is made of striated tissue. These two samples give the highest standard deviations compared to the mean value. The samples of the artery wall were taken from intima and media

layers. These layers are made out of elastic fibers and lamellae disposed between collagen fibers and smooth muscle cells. Nevertheless standard deviations are lower than those of skin and myocardium, which means that coefficients measured at different points are less dispersed. Therefore, cellular structures in the aorta sample are larger than those in the skin and myocardium samples. The general trend from these measurements shows that the attenuation and backscattering coefficients decrease as wavelength increases. This is particularly true for skin, in which the attenuation decreases continuously from 8 mm⁻¹ at 810 nm to 4 mm⁻¹ at 1570 nm. For other samples, attenuation decreases abruptly between 810 and 1330 nm, but this trend is less pronounced between 1330 and 1570 nm, as expected from the results collected by Slainter et al.⁵

It is not easy to deduce from Table 2 which source and which wavelength would give the best OCT images in terms of penetration depth and backscattering. Instead of directly comparing the measured attenuation and backscattering, these coefficients were reintroduced in a simplified form of Eq. (3):

$$\Gamma(z') = \alpha_b \exp(-2\alpha_t z') \frac{T_{GS}^2}{R_{GS}}. \quad (8)$$

The main advantage of proceeding in this manner is that we neglect the aperture effects as they mainly depend on the microscope objectives and thus can be altered independently from the source. The effect of the coherence length is also taken out by removing the $l_c/2$ factor. As a consequence, the $\Gamma(z')$ parameter represents the ratio of the backscattered power at depth z' over the incident power obtained with sources that are free from focusing effects [$A(z'), A_{in}=1$]

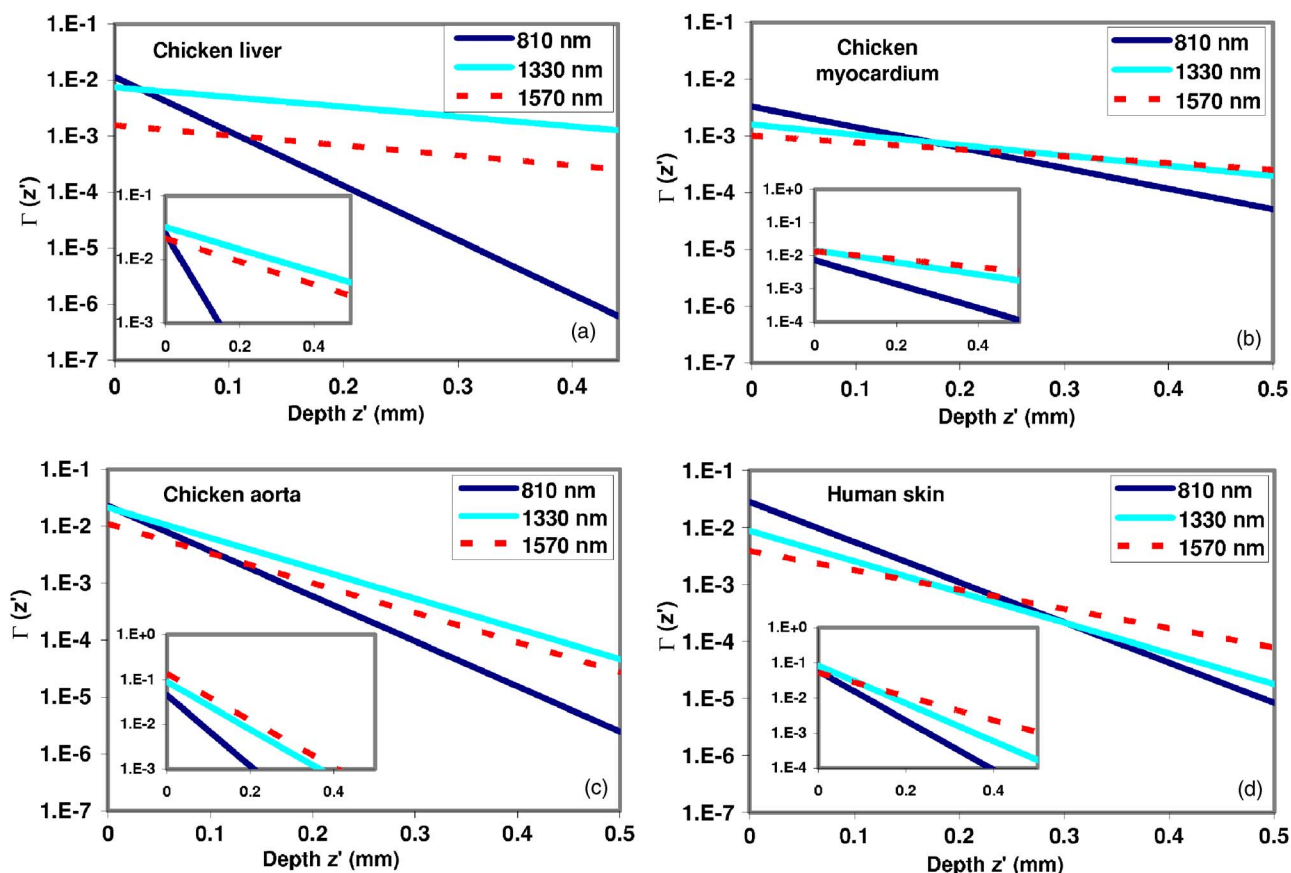


Fig. 5 (a) to (d) Comparison of the parameter $\Gamma(z')$ as a function of depth for several samples at 810-, 1330-, and 1570-nm sources. Inserts in each graph show the case where coherence length is taken into account.

and with equal coherence lengths. Thus, we can establish a clear comparison of the sources only in terms of their emission wavelength. We compare the behavior of $\Gamma(z')$ for each source and for each sample. The results are shown in Fig. 5, where we plot the $\Gamma(z')$ parameter on a logarithmic scale as a function of depth z' . One expects that a low attenuation combined with a high backscattering would give the best performance for OCT imaging. Thus, high values of $\Gamma(z')$ are required to achieve a good SNR. Penetration depths are evaluated by comparing the slopes of the curves in Fig. 5. First, the results show that the 1330-nm broadband source gives the best results for liver and aorta. For shallow depths in human skin and myocardium, the Ti:sapphire laser gives the highest $\Gamma(z')$ values. Nevertheless, as stated by Sainter et al.,⁵ its attenuation is higher than for the 1330- and 1570-nm wavelengths. Surprisingly, the 1570-nm source never gives the highest $\Gamma(z')$ values, except for long depths in human skin. Although the penetration depth at 1570 nm is higher than for the other wavelengths, this result shows that the 1570-nm wavelength is not necessarily the best wavelength for OCT experiments, except in the case of human skin. The assessment made by Bouma et al. that 1500-nm sources are well suited for this type of measurement was based on a qualitative study of penetration depth, but did not include the backscattering amplitude in the comparison.¹⁰ An important limiting factor for 1500-nm sources may be the absorption induced by water inside the tissue and the chamber. As a

matter of fact, water absorption is much more important at 1570 nm (around 0.9 mm^{-1}) than at 1330 nm (around 0.2 mm^{-1}) and at 810 nm, where it is very weak (0.002 mm^{-1}). As a consequence, this factor limits the penetration depth of the 1570-nm SLD much more than the two other sources. Without this limiting factor, the 1570-nm wavelength would give by far the best penetration depths.

Note that these comparisons hold for the emission wavelengths only, and do not take into account the coherence length of each source. Taking into account the $l_c/2$ factor from Eq. (3) and inserting it into Eq. (8) would leave the penetration depth unchanged, but would bring a change in the backreflection amplitude. Subplots to this effect are inserted for each sample in Fig. 5. It turns out that a source with a short coherence length (thus giving a high axial resolution) would give a lower $\Gamma(z')$ parameter and vice versa. The subplots show that for all the samples under test, the 1330-nm source and the SLD benefit from higher $\Gamma(z')$ values compared to the Ti:sapphire laser. This, combined with the high penetration depths already stated, would give a pronounced advantage for these two sources, especially for the SLD in the case of myocardium, skin, and aorta. Still, the 1330-nm source or the Ti:sapphire laser may be chosen in cases where axial resolution takes precedence over the SNR: a coherence length under $10 \mu\text{m}$ is often necessary to obtain high-quality images. Nevertheless, when this condition is achieved, a somewhat larger coherence length may be sometimes prefer-

able because it yields higher backscattering amplitude. As is often the case, trade-offs may be required.

4 Conclusion

The graphical method described in this paper gives a detailed comparison of the OCT performances of these sources and the results emphasize the influence of emission wavelength on penetration depth and backscattering efficiency, on the one hand, and the influence of coherence length, on the other hand. When the coherence length is neglected, our measurements show the advantage of working with 810-nm emission wavelength for good backscattering amplitude and contrast, while sources emitting at 1570 nm give good penetration depth. The 1330-nm sources provide a good compromise between the two. Note that the coherence length can substantially modify the choice of an adequate source in so far as backscattering amplitude can be changed.

Acknowledgments

This work was supported by the Canadian Institute for Photonic Innovations (CIPI) project BP5 and contributions from CIPI Affiliates Bookham Technology and MPB Communications Inc. Other fundings from the CFI and FEMTOTECH programs are also acknowledged.

References

1. D. Huang, E. A. Swanson, C. P. Lin, J. S. Schuman, W. G. Stinson, W. Chang, M. R. Hee, T. Flotte, K. Gregory, K. Puliafito, and J. G. Fujimoto, "Optical coherence tomography," *Science* **254**, 1178–1181 (1991).
2. B. E. Bouma and G. J. Tearney, Eds., *Handbook of Optical Coherence Tomography*, Marcel Dekker, New York (2002).
3. J. M. Schmitt, A. Knüttel, M. Yadlowsky, and M. A. Eckhaus, "Optical-coherence tomography of a dense tissue: statistics of attenuation and backscattering," *Phys. Med. Biol.* **39**, 1705–1720 (1994).
4. Y. Pan and D. L. Farkas, "Noninvasive imaging of living human skin with dual-wavelength optical coherence tomography in two and three dimensions," *J. Biomed. Opt.* **3**, 446–455 (1998).
5. A. W. Sainter, T. A. King, and M. R. Dickinson, "Effect of target biological tissue and choice of light source on penetration depth and resolution in optical coherence tomography," *J. Biomed. Opt.* **9**, 193–199 (2004).
6. J. M. Schmitt, A. Knüttel, and R. F. Bonner, "Measurement of optical properties of biological tissues by low-coherence reflectometry," *Appl. Opt.* **32**, 6032–6042 (1993).
7. R. W. Schafer, R. M. Mersereau, and M. A. Richards, "Constrained iterative restoration algorithms," *Proc. IEEE* **69**, 432–450 (1981).
8. A. C. Akçay, J. P. Rolland, and J. M. Eichenholz, "Spectral shaping to improve the point spread function in optical coherence tomography," *Opt. Lett.* **28**, 1921–1923 (2003).
9. A. K. Popp, M. T. Valentine, P. D. Kaplan, and D. A. Weitz, "Microscopic origin of light scattering in tissue," *Appl. Opt.* **42**, 2871–2880 (2003).
10. B. E. Bouma, L. E. Nelson, G. J. Tearney, D. J. Jones, M. E. Brezinski, and J. G. Fujimoto, "Optical coherence tomographic imaging of human tissue at 1.55 μm and 1.81 μm using Er- and Tm-doped fiber sources," *J. Biomed. Opt.* **3**, 76–79 (1998).
11. Y. T. Pan, R. Birngruber, J. Rosperich, and R. Engelhardt, "Measurement of optical-interaction coefficients of intralipid in visible and NIR range," *Proc. SPIE* **2134**, 354–363 (1994).
12. G. J. Tearney, M. E. Brezinski, J. F. Southern, B. E. Bouma, M. R. Hee, and J. G. Fujimoto, "Determination of the refractive index of highly scattering human tissue by optical coherence tomography," *Opt. Lett.* **20**, 2258–2260 (1995).
13. J. M. Schmitt, A. Knüttel, and M. Yadlowsky, "Confocal microscopy in turbid media," *J. Opt. Soc. Am. A* **A11**, 2226–2235 (1994).
14. T. R. Hillman and D. D. Sampson, "The effect of water dispersion and absorption on axial resolution in ultrahigh-resolution optical coherence tomography," *Opt. Express* **13**, 1860–1874 (2005).
15. J. M. Schmitt, "Speckle in optical coherence tomography," *J. Biomed. Opt.* **4**, 95–105 (1999).
16. A. I. Kholodnykh, I. Y. Petrova, K. V. Larin, M. Motamedi, and R. O. Esenaliev, "Precision of measurement of tissue optical properties with optical coherence tomography," *Appl. Opt.* **42**, 3027–3037 (2003).